DOI: 10.1021/acs.chemmater.6b00580

Millisecond Pulsed Films Unify the Mechanisms of Cellulose Fragmentation

Christoph Krumm[§], Jim Pfaendtner[‡], Paul J. Dauenhauer^{§,*}

[§]University of Minnesota, Department of Chemical Engineering and Materials Science, 421 Washington Ave. SE, Minneapolis, MN U.S.A. 55455.

[‡]University of Washington, Department of Chemical Engineering, 3781 Okanogan Lane NE, Seattle, WA U.S.A. 98195.

ABSTRACT: The mechanism of crystalline cellulose fragmentation has been debated between classical models proposing endchain or intra-chain scission to form short-chain (molten) anhydro-oligomer mixtures and volatile organic compounds. Models developed over the last few decades suggest global kinetics consistent with either mechanism, but validation of the chain-scission mechanism via measured reaction rates of cellulose has remained elusive. To resolve these differences, we introduce a new thermal-pulsing reactor four orders of magnitude faster than conventional thermogravimetic analysis (10⁶ vs. 10² °C/min) to measure the millisecond-resolved evolution of cellulose and its volatile products at 400-550 °C. By comparison of cellulose conversion and furan product formation kinetics, both mechanisms are shown to occur with the transition from chain-end scission to intra-chain scission above 467 °C concurrent with liquid formation comprised of short-chain cellulose fragments.

INTRODUCTION

Cellulose is the most abundant polymer in the world, comprising dietary fiber in prepared food, construction and fire-proofing materials, and up to half of lignocellulosic biomass for conversion to biochemicals, fuels, and materials (e.g. biochar). Semi-crystalline cellulose (Fig. 1A) is a linear homopolymer of glucose residues connected by β -(1-4) linkages which thermally fragment above 300 °C¹ to volatile organic compounds²-7 and aerosols³, forming fuel precursors, food products, and air pollutants in wildfires9-10. For more than six decades, efforts to optimize these applications based on controlled polysaccharide decomposition have debated two alternative global mechanisms of cellulose chemistry, shown in Fig. 1B. By the first mechanism, kinetic models of cellulose conversion developed via thermo-gravimetric analysis (TGA) proposed the existence of an undefined reaction intermediate called 'active cellulose,' from which volatile species derive⁴-11-14. The intermediate has also been referred to as 'intermediate liquid cellulose,' from which volatile species derive⁴-11-14. The intermediate has also been referred to as 'intermediate liquid cellulose'-15, wherein cellulose forms partially depolymerized chains which melt. The transformation of cellulose has been observed via photography¹-6-17, with the melt appearing between 450 and 550 °C as depicted in sequential video frames of Fig. 1C and 1D. Alternatively, a second set of cellulose models propose single-step chemical conversion direct to volatile compounds¹-8-22. However, global lumped models of either type exhibit immense range in kinetic parameters (e.g. activation energy, Ea, of 10 to 63 kcal/mol)²-3 leading to uncertainty as to their relevance to cellulose chemistry.

The lack of clarity from two conflicting types of global models has led to a reinterpretation of direct versus indirect cellulose reaction pathways based on molecular mechanisms. Research efforts have predominately focused on elucidating the primary deconstructing unit of cellulose, which has been proposed as small molecules such as levoglucosan by transglycosylation or glucose by chain-end hydrolysis²⁴⁻²⁶ depicted in Fig. 1B. Reformation of glucose monomers precedes traditional aqueous-phase carbohydrate chemistry to other sugars, furans and small (C1-C4) organic compounds^{21, 27-28}. Alternatively, intra-chain (or 'random') scission produces short-chain oligomer intermediates by numerous mechanisms^{21,25,29-34}, which further decompose to monomers and volatile compounds. Although the energetics of both pathways have been calculated, evidence confirming either one has been difficult to obtain due to the lack of experimental methods to discern hundreds of compounds simultaneously evolving above 500 °C within a few milliseconds.

Difficulty in characterizing the evolution of hundreds of volatile compounds from cellulose results from the mismatch of experimental time scales; cellulose chemistry occurs in milliseconds (10⁻³ s) at 500 °C, while analysis of complex organic mixtures via chromatography requires kiloseconds (10⁻³ s). To address this temporal mismatch, we introduce an experimental microreactor for Pulse-Heated Analysis of Solid Reactions (PHASR) depicted in Fig. 2A. The PHASR reactor heats and cools solid reaction samples on a millisecond time scale in order to control reaction progression, allowing for quantification of vapor, gas, and intermediate products as a function of reaction time[†]. Cellulose films (10-50 µm thick, 50-350 µg) are deposited on a passivated steel resistive heating element (red in Fig. 2B) connected to two copper electrodes protruding into the reactor within a thin channel (green) of flowing helium. The sample is continuously cooled via flowing silicon-based coolant (3 °C), which absorbs heat through a composite layer (Fig. 2B) of a microstructured heat exchanger

(250 μ m), aluminum nitride (250 μ m), and heating element (100 μ m). Current (13 V, <2000 A) is applied to the heating element for rapid heating (10⁶ °C/min), and the resulting temperature is monitored with optical emission spectroscopy (1000 Hz). The temperature is maintained at a set point (350 – 600 °C) via a PID controller (2000 Hz) for reaction durations as short as 10 ms; the cellulose film is then quenched when the power is turned off and the sample rapidly cools to room temperature.

The PHASR reactor enables millisecond compositional analysis of cellulose solid/melt and gas-phase products. Variation of the thermal pulse duration (Fig. 2D) produces both quenched intermediate and vapors/gases at tunable extents of cellulose conversion as depicted in Fig. 2C. Heating and cooling is sufficiently fast to achieve negligible conversion (<3%) during the heating/cooling phases³³. Gas and vapors are analyzed by GC/MS, and the quenched cellulose film is characterized by liquid chromatography. Sequential reactive pulses can then be arranged in order of pulse duration as depicted in Fig. 2E, and the evolution of any one of the numerous volatile products such as furfural, levoglucosan, or glycolaldehyde can be quantified individually (inset, Fig. 2E).

EXPERIMENTAL SECTION

PHASR Reactor. The PHASR (Pulse-Heated Analysis of Solid Reactions) reactor was designed to heat and cool cellulose films in millisecond pulses to temperatures ranging from 375-550 °C in an inert atmosphere. Quantification of volatile products and unreacted material with variable pulse length (quantified using gas and liquid chromatography) led to determination of reaction rates under reaction-limited conditions.

The PHASR reactor assembly consisted of two stainless steel custom-machined blocks (the upper heating block and a lower cooling block) which combine to form the reaction chamber, shown in Supplementary Figures S1 and S2. The heating block contained two copper electrical feedthroughs that transfer uniform electrical current to increase the temperature of the steel heating element, which holds the cellulose sample. The cooling block consisted of a micro-machined heat exchanger (MicroCooling Concepts, P/N: SA-5A) through which a high velocity coolant was pumped to cool the sample. The two reactor halves were sealed together with a custom polytetrafluoroethylene (PTFE) gasket, thereby forming a channel through which helium carrier gas flowed (200 sccm) to rapidly inject volatile products into a GC inlet. To prevent condensation of volatile products, the reactor block was heated via five resistive cartridge heaters.

The PHASR reactor was operated with three sub-systems working in unison: (1) power loop with millisecond PID feedback control, (2) cooling loop with high-flow booster pump, and (3) fully-integrated GC-MS analysis. After a sample was loaded, a PHASR reaction was initiated by the power supply system, which resistively heated the sample to the desired temperature for a pre-determined duration (10 – 2000 ms). The cooling loop flowed high velocity coolant through the heat exchanger such that the sample was rapidly cooled when the power supply shut off. Finally, continuously flowing helium carrier gas directed gas and volatile products from the reactor into the GC inlet.

The power loop consisted of a power supply with integrated 2000 Hz controller (Miyachi-Unitek, P/N: HF-2) and transformer (Miyachi-Unitek P/N: IT-1140-3), which converted 480-volt inlet power to 13-volt direct current up to 2000 amps. Feedback temperature control was achieved with an optical pyrometer with optical light pipe probe (Impac IGA-50-LO Plus), which measured the sample temperature at 1000 Hz, and output a 0-20 milliamp signal, which was converted to 0-10 volt signal for feedback to the power supply controller.

The cooling loop consisted of a circulating chiller bath (Fisher Scientific, Isotemp R20) and a high-flow gear pump (ShurFlo/McMaster Carr, P/N: 4272K21), which increased coolant flow during a PHASR reaction. Due to the high temperatures present during a reaction, a high temperature silicon-based heat transfer fluid (DOW, Syltherm-800) was used to prevent film boiling and enable high heat transfer. The closed-loop system was connected with 3/8-inch copper tubing and stainless steel fittings.

The PHASR system was integrated with an Agilent 7890A gas chromatograph with TCD, FID, switching valve, and Agilent 220 ion trap mass spectrometer. Details of product quantification and identification are outlined in the supplementary information[†]. The PHASR reactor was spliced directly into the stainless steel lines between the helium inlet electronic pressure controller (EPC) and the GC inlet, such that the helium carrier gas flowed through the reactor channel and into the GC inlet. Detailed design of the PHASR reactor, including CAD drawings, additional schematics, and validation techniques is provided in the supplementary information[†].

Cellulose Preparation. Carbohydrate film samples depicted in Figures 1, 2 and 3 were prepared using the thin film deposition method of Mettler et al³⁵. All samples were used as-purchased and exceeded 90% purity. Cellobiose was purchased from Sigma-Aldrich, and larger glucan carbohydrate molecules (DP=3-6) were purchased from Megazyme (P/N G6: O-CHE, G4: O-CTE, G3: O-CTR). Microcrystalline cellulose was purchased from Alfa Aesar (P/N A17730). Previous work has shown that the presence of trace amounts of inorganic impurities such as calcium and magnesium can have a strong effect on high temperature carbohydrate chemistry; however, ICP-MS analysis of cellulose samples used for experiments has shown negligible quantities of inorganic material³⁸.

Heating elements were cleaned prior to experiment using a handheld torch until the metal turned blue, after which the heating elements were allowed to sit for 24 hours. A suspension/solution of the desired feedstock in HPLC grade water (1.0 wt/wt percent) was prepared and stirred for three hours to ensure proper suspension. Aliquots of the suspension/solution (5 μ l, equivalent to 50 μ g sample) were pipetted onto the center of a cleaned heating element to form a droplet 3.0 mm in diameter. The suspension media was evaporated in a vacuum oven at 40 °C at 25 inHg vacuum. To gen-

erate samples with a mass larger than 50 µg, multiple deposition and drying procedures were performed in series, thereby forming a uniform film of constant diameter and tunable thickness. Cellulose film thickness depicted in Figure 3A of the main paper was spatially evaluated via optical profilometry (Keyence VHX-5000 with VH-Z250R optics). Film thickness values displayed in the x-axis in Figure 3B were measured by averaging thickness from three linear profiles across the center of the films. Additional profilometry data is shown in the supplementary information[†].

Carbohydrate Quantification. Quantification of non-volatile carbohydrate content within partially reacted films (Figure 4) was accomplished via solvent extraction and liquid chromatography with light scattering detection. Heating elements with quenched, partially-reacted samples were cut to a smaller size such that they fit in 1.5 mL PTFE filter vials (Whatman, UN203NPEPP) and 300 μl of HPLC grade water was pipetted into each vial. Vials containing heating element pieces and water were sonicated for five minutes to ensure dissolution of soluble compounds, after which the steel heating element, now free of sample, was removed from the vial. The vial filter plunger was then depressed, and 100 μl of sample was injected into an HPLC with a light scattering detector (Shimadzu Prominence with ELSD-LTII) with a carbohydrate separation column (Agilent NA-HiPlex, PL1171-6140) and water mobile phase. α-Cyclodextrin was identified via retention time analysis and quantified via calibration using identical sample preparation methods (i.e. heating element preparation and filtration). Calibrations were performed daily. Initial reaction rates of α-cyclodextrin at different temperatures, as shown in Figure 4 of the main paper, were quantified by measuring the amount of remaining α-cyclodextrin at early reaction times ($X_{\alpha-cyclodextrin} < 20\%$) in partially reacted thin film samples, defined as:

$$r_{\alpha-\text{cyclodex.}} = \frac{(\text{mol } \alpha-\text{cyclodex.consumed})}{(\text{mol } \alpha\text{cyclodex.})*(\text{reaction duration})}$$

A sample liquid chromatogram of α -cyclodextrin is provided in the supplementary information[†].

Visualization. High-speed photography was performed using the top portion of the PHASR reactor mounted upside down to rapidly heat the cellulose film sample. A custom fabricated helium diffuser ring made from ½ inch stainless steel tubing provided an inert environment around the cellulose film. Lighting was provided from an angle using a high power directional light source (Prior, Lumen 200). High speed videos were collected at 1000 frames per second using a high speed camera (Phantom eX-2) with a macro lens. Additional detail, including expanded frames and a schematic of the visualization setup, is provided in the supporting information[†].

RESULTS AND DISCUSSION

Measured reaction rates with thin cellulose films measured via the PHASR reactor are intrinsic chemical reaction rates devoid of heat and mass transfer artifacts or secondary/gas-phase reactions † . As depicted in Fig. 3A, the thickness of cellulose films was varied from 20 μ m to 100 μ m (characterized by optical profilometry), and the formation rate of volatile product species was measured at 500 °C as shown in Fig. 3B. For samples of thickness of 20, 35, 45, and 60 μ m, the formation rate of volatiles was constant, but measured rates decreased monotonically above 70 μ m indicative of the onset of transport limitations in large (>70 μ m) samples.

Using thin, isothermal cellulose films (50 µm), the millisecond temporal evolution of eight major furans (furfural, 5-hydroxymethylfurfural, 2,5-dimethylfuran, 2-methylfuran, 2-furanmethanol, 5-methylfurfural, furan, and 2(5H)-Furanone) was measured within one second. Furans were selected as a class of compounds indicative of volatile organic products; yield of furans in this work measured at complete conversion was in agreement with previous furan yields (7-9 C%) at high carbon balance^{4,33}. As depicted in Fig. 3C, furan formation (with normalized yield) at 500 °C exhibits apparent first order kinetics; the formation rate of furans from cellulose (i.e. slope of the fit line in Fig. 3C) decreases until cellulose is fully converted. However, furan formation at 450 °C exhibited apparent zero order kinetics; the rate of furan(s) formation was independent of the extent of cellulose conversion (Fig. 3E).

The kinetic transition between 450 and 500 °C is amenable to simple cellulose decomposition mechanisms. A fixed product formation rate is consistent with a static concentration of cellulose active sites; as depicted in the inset of Fig. 3E, chain-end depolymerization retains a fixed quantity of chain ends as individual monomeric products dissociate. Alternatively, as the reaction proceeds at 500 °C, a reduction in the formation rate of volatile furan products (i.e. slope of the fit line in Fig. 3C) with time is consistent with consumption of the cellulose active sites; intra-chain 'random' scission breaks inter-monomer glycosidic bonds which are initially plentiful in cellulose.

The mechanisms of intra-chain versus chain-end scission were readily verified by measuring the differential formation rate of furan products (conversion <20%) from varying length short-chain β -(1,4)-cellodextrin reactants (Fig. 3D and 3F). At 550 °C, all cellodextrins exhibit the same furan product formation rate per unit mass independent of chain size; cellulose/cyclodextrin exhibit similar furan formation rates only two or three times slower despite cellulose being longer than cellodextrins by about two orders of magnitude. However, at 400 °C, the rate of furan formation was the same from all cellodextrins only when normalized by the concentration of polymer chains, indicating that product formation occurs only at the cellulose chain end.

The transition between two competing cellulose decomposition mechanisms is evident when comparing the relative rates of cellulose conversion and furan product evolution. As depicted in Fig. 4, the rate of furan formation from cellulose exhibits a distinct transition (i.e. change in slope) at 467 °C, consistent with a change in rate-controlling mechanism. The rate of cellulose conversion (blue in Fig. 4) was determined using α -cyclodextrin as a surrogate, which has been shown to Page 3

exhibit the same products³⁵ and reaction rates (Fig. S₅) as cellulose but is readily characterized via liquid chromatography. A similar transition was also observed at 467 °C with cyclodextrin, which dramatically increases in conversion rate at higher temperatures.

The kinetic transition at 467 °C is interpreted as a 'reactive melting point' (T_{RM}) which is the temperature above which the change in cellulose decomposition chemistry leads to the formation of a melt phase. Below T_{RM} , end-chain scission slowly produces monomer-sized species, which rapidly devolatilize; the overall rate limitation of cellulose chain-end scission is apparent in the absence of a melt phase intermediate and the similar change in rates (i.e. slope in Fig. 4) observed for both cellulose/cyclodextrin conversion and furans formation. However, cyclodextrin decomposition above T_{RM} exhibits first-order kinetics consistent with intra-chain scission (Fig. S8), indicating that cellulose and cyclodextrin decomposition accelerates with increasing temperature and diverges from the furan formation rate as all inter-monomer linkages break. Rapid formation of chain fragment intermediates small enough to melt then accumulate before eventually reacting to volatile species such as furans.

Molecular-level insight gained from millisecond film kinetics unifies two global philosophies of cellulose chemistry. Intra-chain mechanisms above 467 °C lead to the intermediate-controlled mechanisms first proposed by Shafizadehⁿ, while chain-end mechanisms at low temperature lead to direct mechanisms of Broido¹⁸. While the precise chemistry of both polymer mechanisms have yet to be determined, the reaction rates and apparent energetics of Fig. 4[†] measured via PHASR provide verification for the complex mechanisms of cellulose and eventually other polymers such as lignin and hemicellulose at high temperature. From a broader perspective, the two mechanisms of cellulose chemistry above and below T_{RM} have unknowingly directed the development of thermochemical biomass technologies. Cellulose gasification/combustion conducted well above T_{RM} ensures decomposition to small molecules via intra-chain scission, while formation of solid, carbonaceous solids via biocharring or torrefaction occurs below T_{RM} due to slow decomposition via chain-end chemistry of long cellulose chains. Numerous studies of cellulose pyrolysis have identified the moderate temperature of 500 °C as optimal for maximum liquid product yield³⁶⁻³⁷; reactions just above T_{RM} ensure rapid breakdown of cellulose to volatile organic compounds by intra-chain scission without promoting further decomposition to gases.

SUMMARY AND CONCLUSIONS

Fragmentation kinetics of cellulose conversion and volatile furan product formation were measured at 375-550 °C to elucidate the polymer mechanisms leading to solid char and intermediate liquid formation. Cellulose reaction rates were measured using a high temperature reactor called PHASR (Pulsed-Heated Analysis of Solid Reactions), wherein films of cellulose (10-250 μ m) were rapidly heated via electrical resistance, maintained at reaction temperature for a predetermined duration (10 ms to 2.0 s), and then rapidly quenched. The millisecond-resolved evolution of reacting cellulose and evolving volatile products was subsequently characterized by integrated gas chromatography and ex situ liquid chromatography.

Cellulose films 500 °C were shown to react without heat and mass transfer limitations in samples thinner than 70 μ m. For reaction-controlled conditions, inspection of the extent of conversion of cellulose with time indicated that furan formation exhibits zero-order rate dependence at low temperature (T < 467 °C) and first-order rate dependence at high temperature (T > 467 °C). By comparison of the furan product formation rate from short-chain cellodextrins, the mechanism of cellodextrin decomposition was shown to occur by chain-end cleavage at low temperature and intra-chain mechanisms at high temperature. Measurement of differential kinetics of furan formation and cellulose conversion (evaluated with the surrogate α -cyclodextrin) revealed a distinct kinetic transition at 467 °C, consistent with a 'reactive melting point' (T_{RM}) of cellulose

ASSOCIATED CONTENT

†Supporting Information. A detailed description of the experimental technique, associated methods, and data analysis is located in the supporting information section. This material is available free of charge via the Internet at http://pubs.acs.org.

AUTHOR INFORMATION

Corresponding Author

* Paul J. Dauenhauer, Associate Professor of Chemical Engineering and Materials Science, http://dauenhauer.cems.umn.edu/ Email: hauer@umn.edu Twitter: @pauldauenhauer

ACKNOWLEDGMENT

We acknowledge support from the U.S. Department of Energy Early Career Program, Basic Energy Science – Catalysis (DE-SC0012659).

ABBREVIATIONS

PHASR, Pulsed-Heated Analysis of Solid Reactions.

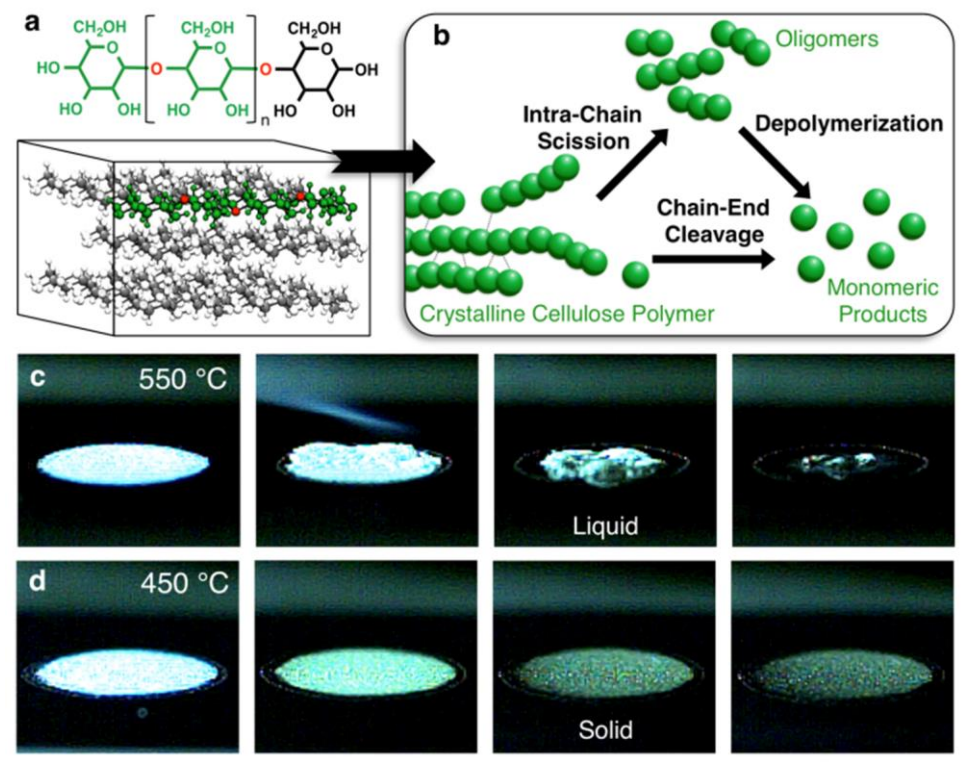


Figure 1. Direct and Indirect Pathways of Cellulose Fragmentation. (A) Cellulose crystal structure (I- β polymorph) with linear glucan polymer chains (carbon atoms in green, inter-monomer oxygens in red). (B) Direct (chain-end cleavage) and indirect (intrachain scission) pathways of cellulose decomposition to monomeric products. (C) Photography of a cellulose film (3.0 mm diameter, thickness of 50 μ m) on a 550 °C surface forming a liquid intermediate before vaporizing. (D) Cellulose film on a 450 °C surface reacts without melting.

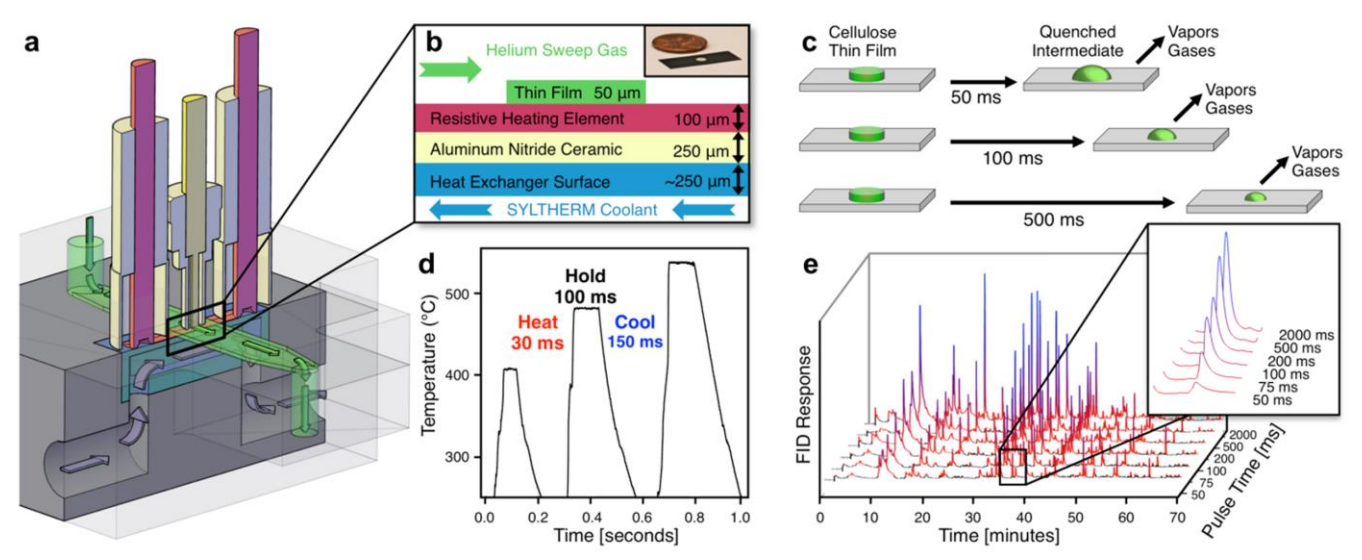


Figure 2. Pulse-Heated Analysis of Solid Reactions (PHASR) Reactor. (A) Cut-away diagram of the PHASR reactor shows resistive heating electrical feedthroughs in mauve, an optical pyrometer for millisecond feedback temperature control in yellow, helium carrier gas flow in green, and coolant flow path in blue. (B) A magnified view of the PHASR reactor with layers which transfer heat to the liquid coolant. (C) Analysis of products from cellulose films heated for variable lengths of time to obtain time-resolved kinetics. (D) Three thermal profiles show rapid heating in fewer than 30 milliseconds and cooling in fewer than 150 milliseconds. (E) Arranged GC-FID chromatograms show the formation of individual pyrolysis species with increasing pulse time.

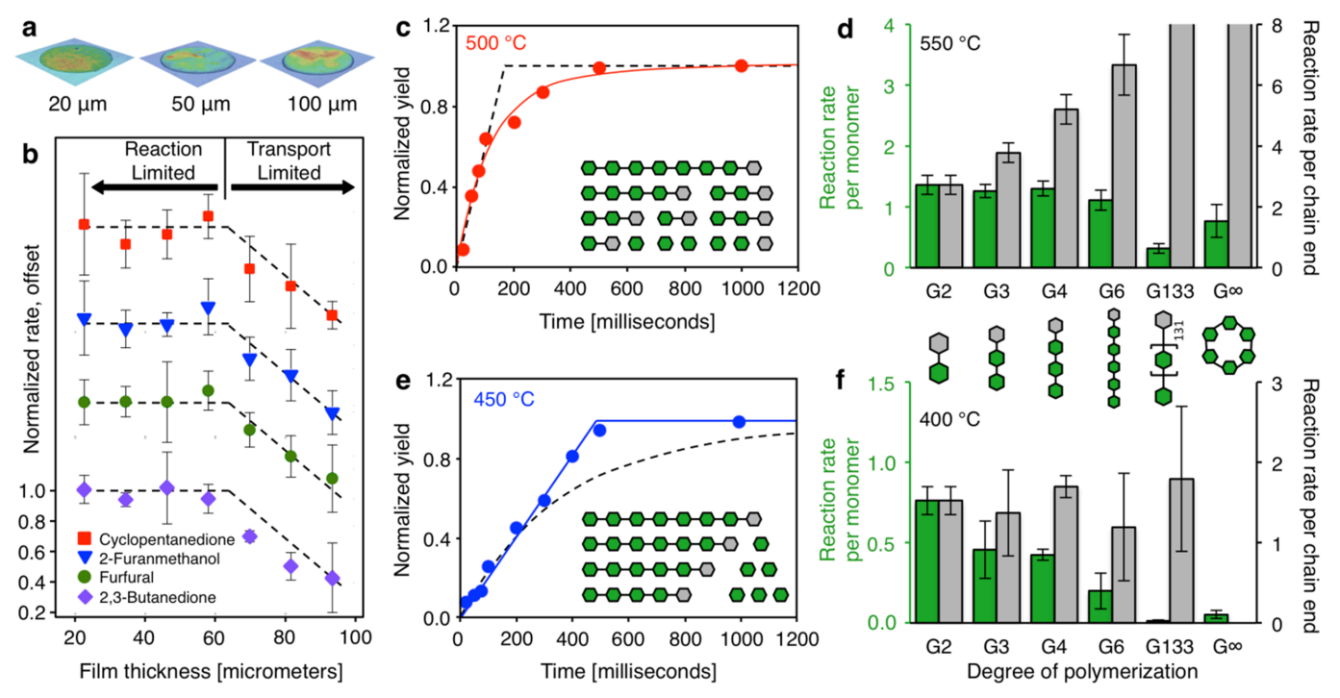


Figure 3. PHASR Kinetics: End-chain and intra-chain fragmentation mechanisms of cellulose. (A) Variable cellulose film thickness characterized by optical profilometry. (B) Differential kinetics of product formation from cellulose at 500 °C for variable film thickness. (C) Time-resolved, normalized yield of eight furan products shows apparent first-order kinetics at high temperature with first-order (red line) and zero-order (black dashes) kinetic models. (D) Differential furans product formation rate per monomer (green bars) or per chain end (grey bars) from cellodextrins (G2-G6), cellulose (G133), and α-cyclodextrin indicates the mid-chain scission mechanism dominates at 550 °C. Reaction rates per chain end are defined as (mol. furans)/(mol. reactant*s) and reaction rates per mol monomer are defined as (mol. furans)/(mol. glucan monomer in reactant*s) (E) Time-resolved, normalized yield of eight furan products exhibits apparent zero-order kinetics at low temperature with zero-order (blue line) and first-order (black dashes) kinetic models. (F) Differential furan product formation rate per monomer (green bars) or per chain end (gray bars) from cellodextrins (G2-G6), cellulose, and α-cyclodextrin indicates the chain-end mechanism dominates at 400 °C.

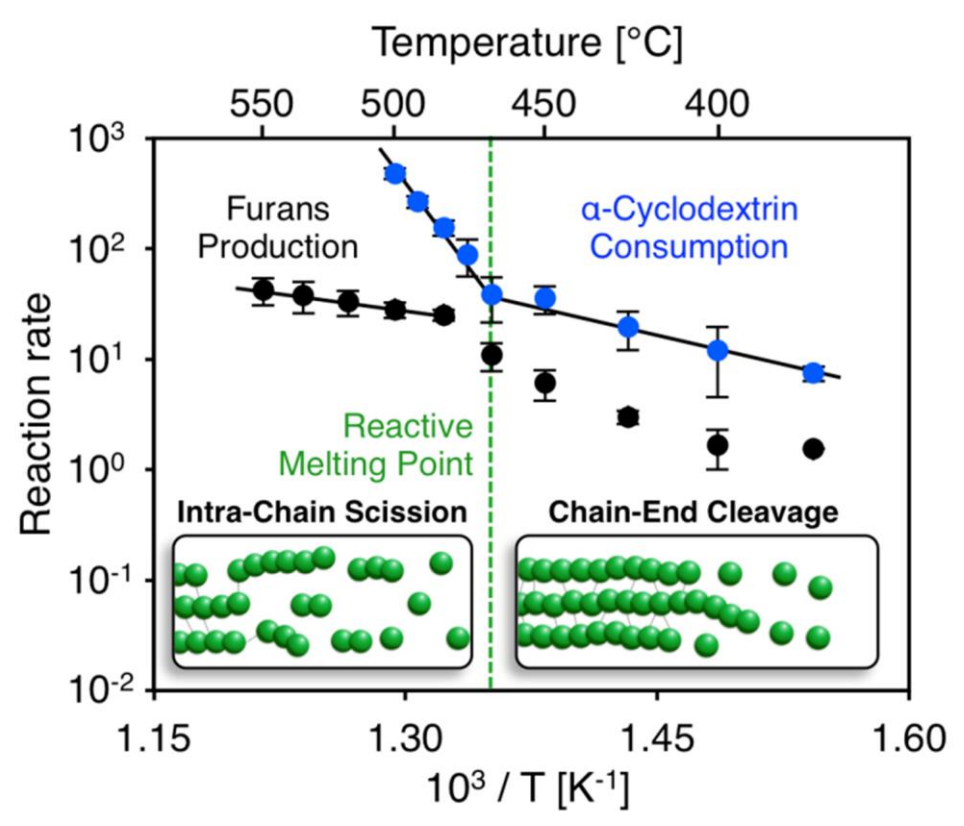


Figure 4. Differential Kinetics of Cellulose Fragmentation Reveal the Reactive Melting Point, T_{RM} . A plot of reaction rate versus inverse temperature for production of furans (black) and consumption of polymer (blue) exhibits a transition from chain-end cleavage to mid-chain scission at T_{RM} of 467 °C, identified by a shift in reaction rates. Above T_{RM} , polymer decomposition is sufficiently fast such that short-chain fragments accumulate as a liquid intermediate, before eventually decomposing to furans. Reaction rates for furans are defined as (mol. furans)/(mol. glucan monomer in reactant*s), while reaction rates for α-cyclodextrin are defined as (mol. α-cyclodextrin consumed)/(mol. α-cyclodextrin reactant*s).

REFERENCES

- (1) Wang, Z.; McDonald, A. G.; Westerhof, R. J. M.; Kersten, S. R. A.; Cuba-Torres, C. M.; Ha, S.; Pecha, B.; Garcia-Perez, M., Effect of cellulose crystallinity on the formation of a liquid intermediate and on product distribution during pyrolysis. *J. Anal. Appl. Pyrolysis* **2013**, *100*, 56-66.
- (2) Stamm, A. J., Thermal Degradation of Wood and Cellulose. Ind. & Eng. Chem. 1956, 48, 413-417.
- (3) Lipska, A. E.; Parker, W. J., Kinetics of the pyrolysis of cellulose in the temperature range 250–300°C. J. Appl. Polym. Sci. 1966, 10, 1439-1453.
- (4) Lin, Y.-C.; Cho, J.; Tompsett, G. A.; Westmoreland, P. R.; Huber, G. W., Kinetics and Mechanism of Cellulose Pyrolysis. *J. Phys. Chem. C* 2009, 113, 20097-20107.
- (5) Patwardhan, P. R.; Satrio, J. A.; Brown, R. C.; Shanks, B. H., Product distribution from fast pyrolysis of glucose-based carbohydrates. *J Anal. Appl. Pyrolysis* 2009, 86, 323-330.
- (6) Di Blasi, C., Modeling chemical and physical processes of wood and biomass pyrolysis. Prog. Energy Combust. Sci. 2008, 34, 47-90.
- (7) Mettler, M. S.; Paulsen, A. D.; Vlachos, D. G.; Dauenhauer, P. J., Pyrolytic conversion of cellulose to fuels: levoglucosan deoxygenation via elimination and cyclization within molten biomass. *Energy Environ. Sci.* **2012**, *5*, 7864-7868.
- (8) Teixeira, A. R.; Mooney, K. G.; Kruger, J. S.; Williams, C. L.; Suszynski, W. J.; Schmidt, L. D.; Schmidt, D. P.; Dauenhauer, P. J., Aerosol generation by reactive boiling ejection of molten cellulose. *Energy Environ. Sci.* 2011, 4, 4306-4321.
- (9) Randerson, J. T.; Liu, H.; Flanner, M. G.; Chambers, S. D.; Jin, Y.; Hess, P. G.; Pfister, G.; Mack, M. C.; Treseder, K. K.; Welp, L. R.; Chapin, F. S.; Harden, J. W.; Goulden, M. L.; Lyons, E.; Neff, J. C.; Schuur, E. A. G.; Zender, C. S., The Impact of Boreal Forest Fire on Climate Warming. *Science* **2006**, 314, 1130-1132.
- (10) Wotawa, G.; Trainer, M., The Influence of Canadian Forest Fires on Pollutant Concentrations in the United States. *Science* **2000**, 288, 324-328.
- (11) Bradbury, A. G. W.; Sakai, Y.; Shafizadeh, F., A kinetic model for pyrolysis of cellulose. J. of Appl. Polym. Sci. 1979, 23, 3271-3280.
- (12) Shafizadeh, F., Introduction to pyrolysis of biomass. J. Anal. and Appl. Pyrolysis 1982, 3, 283-305.
- (13) Piskorz, J.; Radlein, D.; Scott, D. S., On the mechanism of the rapid pyrolysis of cellulose. *J. of Anal. and Appl. Pyrolysis* 1986, 9, 121-137.
- (14) Dufour, A.; Weng, J.; Jia, L.; Tang, X.; Sirjean, B.; Fournet, R.; Gall, H. L.; Brosse, N.; Billaud, F.; Mauviel, G.; Qi, F., Revealing the chemistry of biomass pyrolysis by means of tunable synchrotron photoionisation-mass spectrometry. RSC Adv. 2013, 3, 4786-4792.
- (15) Lédé, J., Cellulose pyrolysis kinetics: An historical review on the existence and role of intermediate active cellulose. J. Anal. Appl. Pyrolysis 2012, 94, 17-32.
- (16) Boutin, O.; Ferrer, M.; Lédé, J., Radiant flash pyrolysis of cellulose—Evidence for the formation of short life time intermediate liquid species. *J. Anal. Appl. Pyrolysis* 1998, 47, 13-31.
- (17) Dauenhauer, P. J.; Colby, J. L.; Balonek, C. M.; Suszynski, W. J.; Schmidt, L. D., Reactive boiling of cellulose for integrated catalysis through an intermediate liquid. *Green Chem.* 2009, 11, 1555-1561.
- (18) Broido, A.; Nelson, M. A., Char yield on pyrolysis of cellulose. Combust. Flame 1975, 24, 263-268.
- (19) Lede, J.; Diebold, J. P.; Peacocke, G. V. C.; Piskorz, J., The Nature and Properties of Intermediate and Unvaporized Biomass Pyrolysis Materials. In *Developments in Thermochemical Biomass Conversion*, Bridgwater, A. V.; Boocock, D. G. B., Eds. Springer Netherlands: 1997; pp 27-42.
- (20) Varhegyi, G.; Jakab, E.; Antal, M. J., Is the Broido-Shafizadeh Model for Cellulose Pyrolysis True? Energy Fuels 1994, 8, 1345-1352.
- (21) Antal, M. J.; Várhegyi, G.; Jakab, E., Cellulose Pyrolysis Kinetics: Revisited. Ind. Eng. Chem. Res. 1998, 37, 1267-1275.
- (22) Antal, M. J., Jr.; Varhegyi, G., Cellulose Pyrolysis Kinetics: The Current State of Knowledge. Ind. Eng. Chem. Res. 1995, 34, 703-717.
- (23) Burnham, A. K.; Zhou, X.; Broadbelt, L. J., Critical Review of the Global Chemical Kinetics of Cellulose Thermal Decomposition. *Energy Fuels* **2015**, *29*, 2906-2918.
- (24) Vinu, R.; Broadbelt, L. J., A mechanistic model of fast pyrolysis of glucose-based carbohydrates to predict bio-oil composition. *Energy Environ. Sci*, 2012, 5, 9808-9826.
- (25) Matsuoka, S.; Kawamoto, H.; Saka, S., What is active cellulose in pyrolysis? An approach based on reactivity of cellulose reducing end. J. Anal. Appl. Pyrolysis 2014, 106, 138-146.
- (26) Matsuoka, S.; Kawamoto, H.; Saka, S., Thermal glycosylation and degradation reactions occurring at the reducing ends of cellulose during low-temperature pyrolysis. *Carbohydr. Res.* **2011**, 346, 272-279.
- (27) Mayes, H. B.; Nolte, M. W.; Beckham, G. T.; Shanks, B. H.; Broadbelt, L. J., The Alpha–Bet(a) of Glucose Pyrolysis: Computational and Experimental Investigations of 5-Hydroxymethylfurfural and Levoglucosan Formation Reveal Implications for Cellulose Pyrolysis. *ACS Sustainable Chem. Eng.* **2014**, 2, 1461-1473.
- (28) Zhou, X.; Nolte, M. W.; Mayes, H. B.; Shanks, B. H.; Broadbelt, L. J., Experimental and Mechanistic Modeling of Fast Pyrolysis of Neat Glucose-Based Carbohydrates. 1. Experiments and Development of a Detailed Mechanistic Model. *Ind. Eng. Chem. Res.* 2014, 53, 13274-13289.
- (29) Mayes, H. B.; Broadbelt, L. J., Unraveling the Reactions that Unravel Cellulose. J. Phy. Chem. A 2012, 116 (26), 7098-7106.
- (30) Agarwal, V.; Dauenhauer, P. J.; Huber, G. W.; Auerbach, S. M., Ab Initio Dynamics of Cellulose Pyrolysis: Nascent Decomposition Pathways at 327 and 600 °C. *J. Am. Chem. Soc.* **2012**, *134*, 14958-14972.
- (31) Zhang, Y.; Liu, C.; Chen, X., Unveiling the initial pyrolytic mechanisms of cellulose by DFT study. *J. Anal. Appl. Pyrolysis* **2015**, *113*, 621-629.
- (32) Assary, R. S.; Curtiss, L. A., Thermochemistry and Reaction Barriers for the Formation of Levoglucosenone from Cellobiose. *ChemCatChem* **2012**, 4, 200-205.
- (33) Hosoya, T.; Nakao, Y.; Sato, H.; Kawamoto, H.; Sakaki, S., Thermal Degradation of Methyl β -d-Glucoside. A Theoretical Study of Plausible Reaction Mechanisms. *J. Org. Chem.* **2009**, *74*, 6891-6894.
- (34) Hosoya, T.; Sakaki, S., Levoglucosan Formation from Crystalline Cellulose: Importance of a Hydrogen Bonding Network in the Reaction. *ChemSusChem* **2013**, *6*, 2356-2368.

- (35) Mettler, M. S.; Mushrif, S. H.; Paulsen, A. D.; Javadekar, A. D.; Vlachos, D. G.; Dauenhauer, P. J., Revealing pyrolysis chemistry for biofuels production: Conversion of cellulose to furans and small oxygenates. *Energy Environ. Sci.* **2012**, *5*, 5414-5424.
- (36) Bridgwater, A. V., Review of fast pyrolysis of biomass and product upgrading. Biomass Bioenergy 2012, 38, 68-94.
- (37) Kersten, S.; Garcia-Perez, M., Recent developments in fast pyrolysis of ligno-cellulosic materials. *Curr. Opin. Biotechnol.* **2013**, 24, 414-420.
- (38) Zhu. C.; Maduskar, S.; Paulsen, A.D.; Dauenhauer, P.J., Alkaline Earth Metal Catalyzed Thin-Film Pyrolysis of Cellulose. 2016 *ChemCatChem*. DOI: 10.1002/cctc.201501235